

## A study of warm rain detection using A-Train satellite data

Ruiyue Chen,<sup>1,2</sup> Zhanqing Li,<sup>2,3</sup> Robert J. Kuligowski,<sup>4</sup> Ralph Ferraro,<sup>5</sup>  
and Fuzhong Weng<sup>3</sup>

Received 23 November 2010; revised 23 December 2010; accepted 3 January 2011; published 18 February 2011.

[1] Warm rain occurs in low-level liquid water clouds and does not involve an ice-phase process. Comprising many state-of-the-art passive and active instruments, the NASA A-Train series of satellites provide comprehensive simultaneous information about warm clouds and their precipitation processes. This study exploits multi-sensor data from the A-Train satellite constellation to investigate the rain contribution from warm clouds and the potential of using cloud microphysical parameters for warm rain detection. It is shown that warm rain accounts for a significant portion of total precipitation over the global ocean. Cloud microphysical parameters (e.g., liquid water path) show potential for detecting warm rain events and estimating the rain rates. Key parameters for estimating warm rain using cloud microphysical parameters are also examined. **Citation:** Chen, R., Z. Li, R. J. Kuligowski, R. Ferraro, and F. Weng (2011), A study of warm rain detection using A-Train satellite data, *Geophys. Res. Lett.*, 38, L04804, doi:10.1029/2010GL046217.

### 1. Introduction

[2] Precipitation estimates are valuable for flood forecasting, numerical weather prediction, and climate modeling. Satellite data have been widely used to estimate global precipitation. Instruments on board satellites for precipitation estimation include passive microwave radiometers, infrared (IR) imagers, and cloud/precipitation radars.

[3] Passive microwave radiometer measurements of low-frequency emissions are widely used to estimate precipitation over oceans because of the direct influence of hydrometeors on microwave radiances over ocean surfaces [e.g., *Wilheit et al.*, 2003]. However, such algorithms are not applicable over land because of the highly variable and often unknown surface emissivity. Over land, the attenuation of surface emission by cloud ice particles at high frequency channels (i.e., 85 GHz) is used to estimate the precipitation rate.

[4] Passive microwave instruments are generally aboard low-altitude polar-orbiting satellites, which observe a particular mid-latitude location twice a day at most and observation gaps exist over the Tropics. IR and near-IR instruments on geostationary satellites provide continuous

high-resolution cloud observations, which are used in many studies for continuous rainfall monitoring over specific regions. IR-based techniques generally rely on cloud-top brightness temperatures and are sometimes calibrated against passive microwave retrievals [e.g., *Kuligowski*, 2002].

[5] Most previous studies on precipitation estimation with satellite data focus on rain involving ice processes, so many algorithms have problems detecting warm rain. IR rain detection algorithms generally fail to detect precipitation from warm clouds because of low thermal contrast. Furthermore, microwave techniques cannot detect warm rain over land since they rely on ice scattering. Over oceans, microwave techniques may underestimate warm rain because it takes place in shallow cloud systems and has a much weaker emission signal than that generated in deeper convective cloud systems.

[6] NOAA's new generation GOES-R satellite is scheduled to be launched in 2015. The proposed Advanced Baseline Imager (ABI) on GOES-R will be used to estimate precipitation operationally. To improve the detection and estimation of warm rain from the ABI, data from NASA's A-Train satellite constellation is used in this study to investigate the rain contribution from warm clouds and the potential for using cloud microphysical parameters for estimating warm rain. The CloudSat cloud profiling radar (CPR) rain rate product, which is part of the A-train satellite data set, is the first dataset that provides warm rain estimates globally. By analyzing two months' worth of data from the MODerate resolution Infrared Spectroradiometer (MODIS) and the Advanced Microwave Scanning Radiometer-Earth Observing System (AMSR-E) on the Aqua satellite and the CPR on the CloudSat satellite, we determine the percentage of rain that is from warm clouds and evaluate the performance of space-borne passive microwave estimates of warm rain over oceans. The potential application of cloud microphysical parameters to warm rain estimation is studied with MODIS estimates of cloud microphysical parameters and coincident CloudSat CPR warm rain estimates.

### 2. Data and Methods

[7] This study uses the Aqua MODIS cloud product, the Aqua AMSR-E rain rate product, and the CloudSat CPR precipitation product. Because the CPR is a nadir-view instrument, only cloud samples along the nadir position of the A-Train satellites' track are used. The study is also limited to cases over oceans between 70°S and 70°N.

[8] The following MODIS cloud products (MOD06) [*King et al.*, 2003] are used in this study: cloud optical depth (TAU), cloud droplet effective radius (DER), cloud liquid water path (CLWP), and cloud-top brightness temperature (T). The spatial resolution is 1-km × 1-km for TAU, DER,

<sup>1</sup>STAR, NESDIS, I.M. System Group at NOAA, Camp Springs, Maryland, USA.

<sup>2</sup>Department of Atmospheric and Oceanic Sciences, University of Maryland, College Park, Maryland, USA.

<sup>3</sup>College of Global Change and Earth System Science, Beijing Normal University, Beijing, China.

<sup>4</sup>Center for Satellite Applications and Research, NESDIS, NOAA, Camp Springs, Maryland, USA.

<sup>5</sup>Center for Satellite Applications and Research, NESDIS, NOAA, College Park, Maryland, USA.

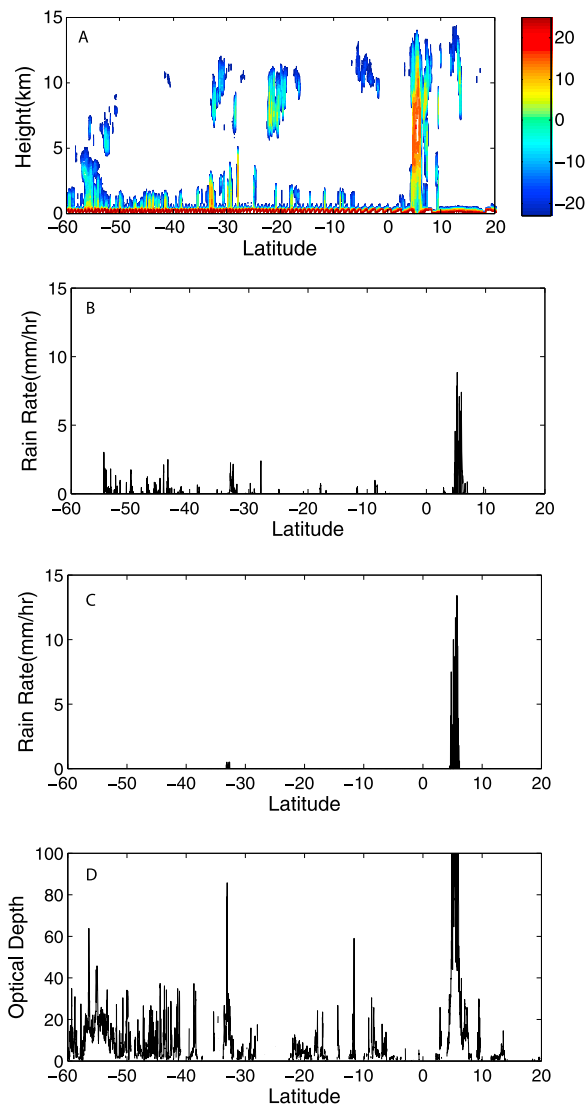


**Figure 1.** A-Train satellite observations during 20:55–21:35 UTC on January 6, 2008: (a) CloudSat CPR reflectivity profiles; (b) CloudSat CPR rain rate estimates; (c) Aqua AMSR-E rain rate estimates; (d) Aqua MODIS cloud optical depth estimates.

and CLWP and the spatial resolution is  $5 \text{ km} \times 5 \text{ km}$  for T. To avoid ice contamination,  $T > 273 \text{ K}$  ( $0^\circ\text{C}$ ) is used as the threshold to identify warm clouds.

[9] CloudSat was launched in April 2006 and carries the first space-borne millimeter wavelength radar for observing atmospheric hydrometeor profiles [Stephens *et al.*, 2008]. The 94-GHz CPR is a W-band, nadir-pointing radar system with a horizontal field-of-view of  $1.7 \text{ km} \times 1.3 \text{ km}$ . Assuming rain rate is constant vertically, the reflectivity near the surface (the forth bin above surface) and the path-integrated attenuation are utilized to estimate rain rate in the CPR 2C - PRECIP-COLUMN product [Haynes *et al.*, 2009]. Because of the surface contamination, CloudSat CPR misses warm rains with very low top height (e.g., less than 1 km).

[10] The AMSR-E L2B rain product [Adler *et al.*, 2007] provides instantaneous rain rate estimates which are derived from AMSR-E microwave brightness temperature observations. The AMSR-E precipitation product uses re-sampled

brightness temperature (BT) data at multiple channels from 6.9 GHz to 89 GHz and has a resolution of 5.4 km. In this study, MODIS estimates of cloud parameters and CPR precipitation estimates are matched to the AMSR-E 5.4-km resolution in the along-track direction.

[11] Figure 1 shows CPR reflectivity profiles, CPR rain rate estimates, AMSR-E rain rate estimates, and MODIS cloud optical depth estimates during the period of 20:55–23:35 UTC January 6 2008 over the eastern Pacific. The CPR reflectivity profiles show two types of rain: from warm, shallow stratocumulus clouds over the Southern Hemisphere and from a deep convective system at  $6^\circ\text{N}$ . The cloud-top heights for the warm-cloud raining areas range between 2 km and 5 km. In Figure 1b, the maximum rain rate estimated by the CPR is around  $2 \text{ mm hr}^{-1}$  for warm rain. In Figure 1c, the AMSR-E rain rate estimates indicate that most warm rain is not detected by the AMSR-E. Figure 1d shows that the MODIS cloud optical depth estimates are well-correlated with the CPR warm rain estimates, but are saturated for the deep convective system.

[12] The cloud/rain observations in Figure 1 indicate that cloud microphysical parameters estimated by visible/near-IR instruments have some potential to estimate warm rain. To explore this, collocated AMSR-E and CPR rain rate products, and MODIS cloud microphysical parameter estimates for low-level liquid cloud samples during January and July 2008 are analyzed in the following sections.

### 3. Results

#### 3.1. Rain Contribution by Clouds With Top Temperatures Greater Than $0^\circ\text{C}$

[13] This study uses CloudSat CPR rain rate estimates and MODIS cloud-top brightness temperature estimates to cal-

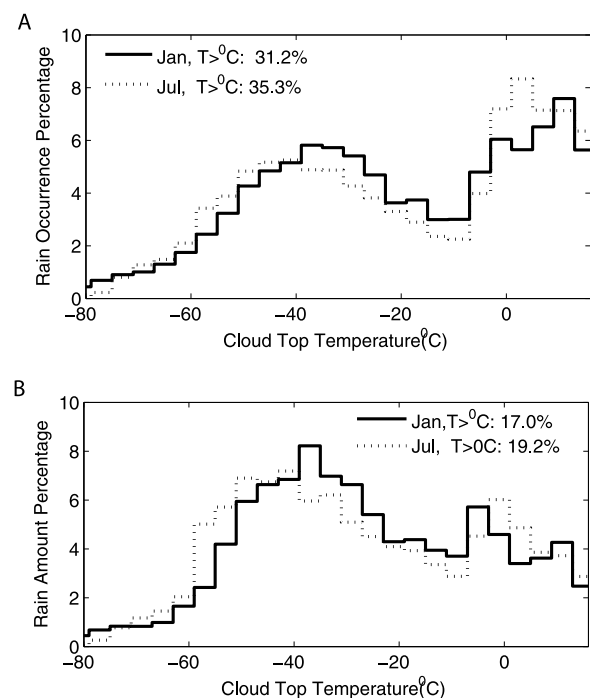


**Figure 2.** Percentage contributions to total rain (a) occurrence and (b) volume as a function of cloud-top brightness temperature.

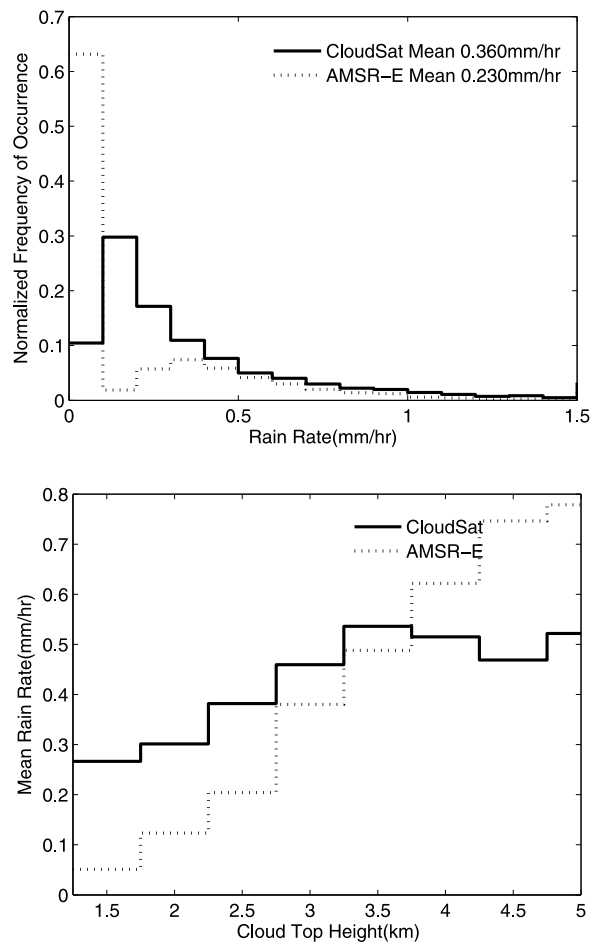


**Figure 3.** Comparison between AMSR-E warm rain rate estimates and CPR warm rain rate estimates for January 2008. (top) Probability density functions. (bottom) Mean rain rate for different cloud top heights.

culate the rain contributions for clouds with different top temperatures. Figure 2a shows the percentage contribution of different cloud top temperatures to total rainfall frequency. The rain rate threshold for the definition of rain occurrence is  $0.05 \text{ mm hr}^{-1}$ . The bimodal distribution shown in Figure 2a is probably the result of the high occurrences of high-level clouds produced by synoptic weather systems and low boundary layer clouds, which are shown in previous studies by both model simulation and satellite global observations [Chang and Li, 2005]. Over the global oceans, the rain from cloud tops warmer than  $0^\circ\text{C}$  encompassed 31.2% of total rain occurrences in January 2008 and 35.3% in July 2008. Figure 2b shows the percentage of the rain volume accounted for by clouds with different cloud-top brightness temperatures. Though warm rains generally have a smaller accumulation than rain events involving ice processes, they contributed 17.0% of the total rain amount over the global oceans in January 2008 and 19.2% in July 2008. It should be noted that the  $0^\circ\text{C}$  threshold for cloud-top brightness temperatures eliminates instances of low-level clouds underneath high-level clouds. Chang and Li [2005] found that over oceans, 36% of low-level clouds are located below cirrus clouds. Therefore, the contribution of warm rain to total rainfall would be much greater than

shown above if low-level clouds in multi-layer cloud systems were included.

### 3.2. Comparisons Between AMSR-E and CPR Warm-Cloud Rain Rate Estimates

[14] Figure 3 (top) shows the distributions of CPR and AMSR-E rain rate estimates for clouds with tops warmer than  $0^\circ\text{C}$  and rain occurrences larger than  $0.05 \text{ mm/hr}$  for January 2008. The average rain rate for all selected clouds is  $0.36 \text{ mm/hr}$  and  $0.23 \text{ mm/hr}$  from the CPR rain estimates and AMSR-E rain estimates, respectively, so compared with the CPR estimates, the AMSR-E underestimates warm-rain rate by 36.2%. Over oceans, passive microwave techniques use observed brightness temperatures to estimate the rain rate because the emission of hydrometers along the view path contributes to the observed brightness temperatures. However, the rain rate is defined as the amount of liquid water that falls to surface per unit area per unit time. Because warm rains are produced by low-level clouds, the observed brightness temperature for warm-cloud rainfall could be much less than that for deeper rain systems, even if the two systems generate the same rain rates. Previous algorithms for rain rate estimation with satellite passive microwave observations mainly focus on deep cloud systems. Therefore, warm rain is often missed or underestimated by these algorithms because of its relatively low contribution to observed brightness temperatures. Figure 3 (bottom) shows the mean rain rates estimated by AMSR-E and CPR for different CPR cloud-top heights during the period of January 2008. AMSR-E significantly underestimates the rainfall rate with respect to the CPR for cloud-top heights below 3.5 km; above that level, AMSR-E overestimates somewhat. Compared with the CPR rain rate estimates, the AMSR-E rain rate estimates are much more highly correlated with cloud top heights, suggesting many high-rate warm rains estimated by AMSR-E are actually from relatively deep clouds. The results for July 2008 are generally consistent with those from January 2008, except that AMSR-E shows even more significant underestimation of warm rain in July (50.1% versus 36.2%). Though AMSR-E operational algorithm [Wilheit *et al.*, 2003] uses re-sampled BT data at multiple channels from 6.9 GHz to 89 GHz and outputs instantaneous rain rate at 5.4 km resolution, the physical footprint sizes are actually different at different AMSR-E channels. Over oceans, AMSR-E is most sensitive to the light warm rain (e.g.,  $0\text{--}2 \text{ mm/hr}$ ) at 37 GHz channel, followed by 19 GHz [Wilheit *et al.*, 2003]. To understand the impacts of large AMSR-E footprint sizes at low frequency channels on the comparisons, CPR warm rain estimates are matched to the along-track direction AMSR-E footprint sizes at 37 GHz and 19 GHz, which are 14 km and 27 km respectively. For January 2008, the underestimation of warm rain by AMSR-E is 33.5% if 14 km is used and is 26.6% if 27 km is used.

### 3.3. The Potential of the Use of Cloud Microphysical Parameters for Warm-Cloud Rain Estimation

[15] Some previous studies [Ba and Gruber, 2001] found that the detection of warm rain can be improved by utilizing cloud observations from the visible and near-IR channels. However, because of the lack of global warm rain observations, few studies have been conducted concerning relationships between cloud microphysical parameters and

**Table 1.** Statistical Relationships Between Cloud Parameters and Warm Rain for January and July 2008<sup>a</sup>

	Raining Threshold		Optimal HSS		Correlation	
	January	July	January	July	January	July
DER( $\mu\text{m}$ )	18.369	19.450	0.172	0.236	0.088	0.161
TAU	16.887	16.973	0.463	0.400	0.363	0.448
LWP(mm)	0.187	0.180	0.524	0.500	0.434	0.530
T( $^{\circ}\text{C}$ )	10.280	11.180	0.055	0.071	0.009	-0.060

<sup>a</sup>HSS is Heidke Skill Score. Only raining cloud samples are used to calculate the correlation coefficients.

warm-cloud rain. To find relationships between warm rain and its associated cloud parameters, we analyzed MODIS estimates of cloud microphysical parameters and coincident CPR rain estimates for low-level liquid water clouds. A  $0.05 \text{ mm hr}^{-1}$  threshold for the CPR rain rate estimate is used to separate raining from non-raining situations. The cloud-top brightness temperatures of the selected cloud samples are required to be higher than  $0^{\circ}\text{C}$ . The potential of cloud parameters for estimating warm rain are discussed in terms of rain/no-rain screening and estimating rain rate. The potential for estimating rain rate is evaluated by the correlation coefficients between MODIS estimates of cloud parameters and CPR estimates of warm-cloud rain rate. The potential of different MODIS-based predictors for rain/no-rain screening are evaluated using the optimal Heidke Skill Score (HSS). HSS is computed by comparing the rain/no-rain screening using MODIS cloud microphysical parameters with the rain/no-rain condition found by the CPR observations:

$$HSS = \frac{2(c_1c_4 - c_2c_3)}{(c_1 + c_2)(c_2 + c_4) + (c_3 + c_4)(c_1 + c_3)}, \quad (1)$$

where  $c_1$  is the number of correct no-rain detections,  $c_2$  is the number of incorrect rain detections,  $c_3$  is the number of incorrect no-rain detections, and  $c_4$  is the number of correct rain detections.

[16] Table 1 shows the statistical relationships between MODIS estimates of cloud parameters and CPR warm rain estimates for January 2008 and July 2008. For January 2008, the highest value of optimal HSS for differentiating raining clouds from non-raining clouds and the best correlation with warm-cloud rain rate is seen for the LWP cloud parameter, followed by TAU and DER, with T far behind. The cloud-top brightness temperature, which has been used in the traditional IR rain detection technique, does not show any potential for warm rain detection. Similar calculations for July 2008 are generally consistent with those from January 2008, except that the prediction skill of TAU and LWP is even higher than for January.

[17] Droplet growth for warm rain is mainly controlled by the coalescence process within a cloud [Stephens and Haynes, 2007]. Cloud optical depth is defined by

$$\tau = \int \int Q_e n(r) \pi r^2 dr dz, \quad (2)$$

where  $n(r)$  is the droplet number distribution,  $z$  is the altitude,  $r$  is the droplet radius, and  $Q_e$  is the extinction efficiency. A cloud with large optical depth is generally thick

and contains more cloud droplets. Cloud optical depth is correlated with warm rain because an optically thicker cloud generally has a longer path and more liquid water for sustaining the coalescence process. DER ( $r_e$ ) is correlated with warm rain because the presence of large droplets (e.g.,  $r > 20 \mu\text{m}$ ) is critical for initiating the coalescence. Using MODIS/CloudSat observations and model simulations, Suzuki *et al.* [2010] found that the raindrop collection efficiency increases with droplet effective radius. LWP denotes total amount of liquid water that could precipitate as warm rain which is computed as [King *et al.*, 2003]

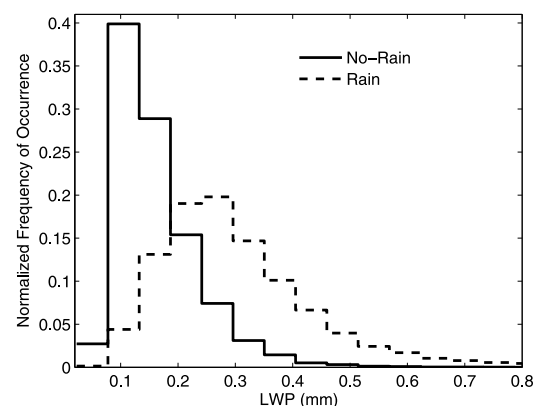
$$LWP = \frac{2}{3} \tau r_e \quad (3)$$

As a combined variable of TAU and DER, LWP has the best merit in detecting warm rain and estimating warm-rain rate. Note that both cloud optical depth and LWP are path-integrated quantities, while MODIS estimates of effective radius are significantly weighted toward cloud top because of the cloud absorption of the near-IR signal [King *et al.*, 2003]. Considering that path integrated attenuation is used in the CPR warm estimates, the path integration characteristics may partially explain their better correlations with the CPR warm rain estimates than the effective radius does. The finding that marine warm clouds with larger LWP are more likely to produce rain has been suggested in previous studies [Stephens and Haynes, 2007; Lebsock *et al.*, 2008; L'Ecuyer *et al.*, 2009].

[18] Figure 4 shows the distribution of LWP for raining clouds and non-raining clouds for January 2008. It is shown that cloud with large LWP (i.e., larger than  $0.187 \text{ mm}$ ) is more likely to be raining, while cloud with small LWP (i.e., less than  $0.187 \text{ mm}$ ) is more likely to be non-raining.

#### 4. Summary

[19] This study analyzed the AMSR-E rain rate estimates, CPR rain rate estimates, and the MODIS estimates of cloud microphysical parameters for low-level liquid water cloud samples collected during January and July of 2008. Over the global oceans, rain from single-layer warm clouds (top temperature  $>0^{\circ}\text{C}$ ) comprised 31.2% (35.3%) of rain occurrences and 17.0% (19.2%) of total rain volume for January (July) 2008. Because of many low-level liquid water

**Figure 4.** Distribution of MODIS LWP for raining clouds and non-raining clouds.

clouds beneath high clouds that are not accounted for in these numbers, the actual contribution of warm rain is probably even larger.

[20] The IR techniques miss all warm-cloud rain because they rely on cloud-top brightness temperature; even passive microwave (AMSR-E) techniques significantly underestimate warm rain, and most of the underestimations occur for clouds with low tops (e.g., lower than 3.5 km). Consequently, the potential of using cloud microphysical parameters in warm rain estimation is investigated. LWP is found to have the best potential for warm rain detection and warm-rain rate estimation. The findings of this study have implications for developing the operational precipitation algorithm for the future GOES-R which employs the Self-Calibrating Multivariate Precipitation Retrieval (SCaMPR) algorithm [Kuligowski, 2002]. Based on the findings of this study we are trying to enhance the SCaMPR to improve the detection and rate estimation of warm rain using GOES-R data. In this study, we examined the relationships of warm rain with each individual cloud parameter. In the future, we will try to develop a algorithm to better estimate warm rain rate using a combination of cloud parameters.

[21] **Acknowledgments.** The authors express their appreciation to the valuable comments from the reviewers. The authors are grateful to the Goddard DAAC for providing the Aqua MOD06 cloud product, to the National Snow and Ice Data Center for providing the Aqua AMSR-E rain product, and to the NASA CloudSat project for providing the CloudSat CPR rain product. This study is supported by NOAA's GOES-R Risk Reduction Program and the GOES-Algorithm Working Group. The contents of this paper are solely the opinions of the authors and do not constitute a statement of policy, decision, or position on behalf of the GOES-R Program Office, NOAA, or the U.S. Government.

## References

- Adler, R., T. Wilhelm Jr., C. Kummerow, and R. Ferraro (2007), AMSR-E/Aqua L2B Global Swath Rain Rate/Type GSFC Profiling Algorithm V002, digital media, Natl. Snow and Ice Data Cent., Boulder, Colo.
- Ba, M., and A. Gruber (2001), GOES Multispectral Rainfall Algorithm (GMSRA), *J. Appl. Meteorol.*, *40*, 1500–1514, doi:10.1175/1520-0450(2001)040<1500:GMRAG>2.0.CO;2.
- Chang, F. L., and Z. Li (2005), A near-global climatology of single-layer and overlapped clouds and their optical properties retrieved from Terra/MODIS data using a new algorithm, *J. Clim.*, *18*, 4752–4771, doi:10.1175/JCLI3553.1.
- Haynes, J. M., T. S. L'Ecuyer, G. L. Stephens, S. D. Miller, C. Mitrescu, N. B. Wood, and S. Tanelli (2009), Rainfall retrieval over the ocean with spaceborne W-band radar, *J. Geophys. Res.*, *114*, D00A22, doi:10.1029/2008JD009973.
- King, M. D., W. P. Menzel, Y. J. Kaufman, D. Tanre, B. C. Gao, S. Platnick, S. A. Ackerman, L. A. Remer, R. Pincus, and P. A. Hubanks (2003), Cloud and aerosol properties, precipitable water, and profiles of temperature and humidity from MODIS, *IEEE Trans. Geosci. Remote Sens.*, *41*, 442–458, doi:10.1109/TGRS.2002.808226.
- Kuligowski, R. J. (2002), A self-calibrating real-time GOES Rainfall algorithm for short-term rainfall estimates, *J. Hydrometeorol.*, *3*, 112–130, doi:10.1175/1525-7541(2002)003<0112:ASCRGT>2.0.CO;2.
- Lebsack, M. D., G. L. Stephens, and C. Kummerow (2008), Multisensor satellite observations of aerosol effects on warm clouds, *J. Geophys. Res.*, *113*, D15205, doi:10.1029/2008JD009876.
- L'Ecuyer, T. S., W. Berg, J. Haynes, M. Lebsack, and T. Takemura (2009), Global observations of aerosol impacts on precipitation occurrence in warm maritime clouds, *J. Geophys. Res.*, *114*, D09211, doi:10.1029/2008JD011273.
- Stephens, G. L., and J. M. Haynes (2007), Near global observations of the warm rain coalescence process, *Geophys. Res. Lett.*, *34*, L20805, doi:10.1029/2007GL030259.
- Stephens, G. L., et al. (2008), CloudSat mission: Performance and early science after the first year of operation, *J. Geophys. Res.*, *113*, D00A18, doi:10.1029/2008JD009982.
- Suzuki, K., T. Y. Nakajima, and G. L. Stephens (2010), Particle growth and drop collection efficiency of warm clouds as inferred from joint CloudSat and MODIS observations, *J. Atmos. Sci.*, *67*, 3019–3032, doi:10.1175/2010JAS3463.1.
- Wilheit, T., C. Kummerow, and R. Ferraro (2003), Rainfall algorithms for AMSR-E, *IEEE Trans. Geosci. Remote Sens.*, *41*, 204–214, doi:10.1109/TGRS.2002.808312.

R. Chen and Z. Li, Department of Atmospheric and Oceanic Sciences, University of Maryland, College Park, MD 20742, USA. (zli@atmos.umd.edu)

R. Ferraro, Center for Satellite Applications and Research, NESDIS, NOAA, 5825 University Research Ct., College Park, MD 20740, USA.

R. J. Kuligowski, Center for Satellite Applications and Research, NESDIS, NOAA, 5200 Auth Rd., Camp Springs, MD 20746-4304, USA.

F. Weng, College of Global Change and Earth System Science, Beijing Normal University, Beijing, China.